UCRL-JC-131658
Preprint

Elastic Constants of β-HMX and Tantalum, Equations of State of Supercritical Fluids and fluid Mixtures and Thermal Transport Determinations

Joseph M. Zaug

This paper was prepared for submittal to
Eleventh International Detonation (1998) Symposium
Snowmass, CO
Aug. 31-Sept. 4, 1998

August 21, 1998

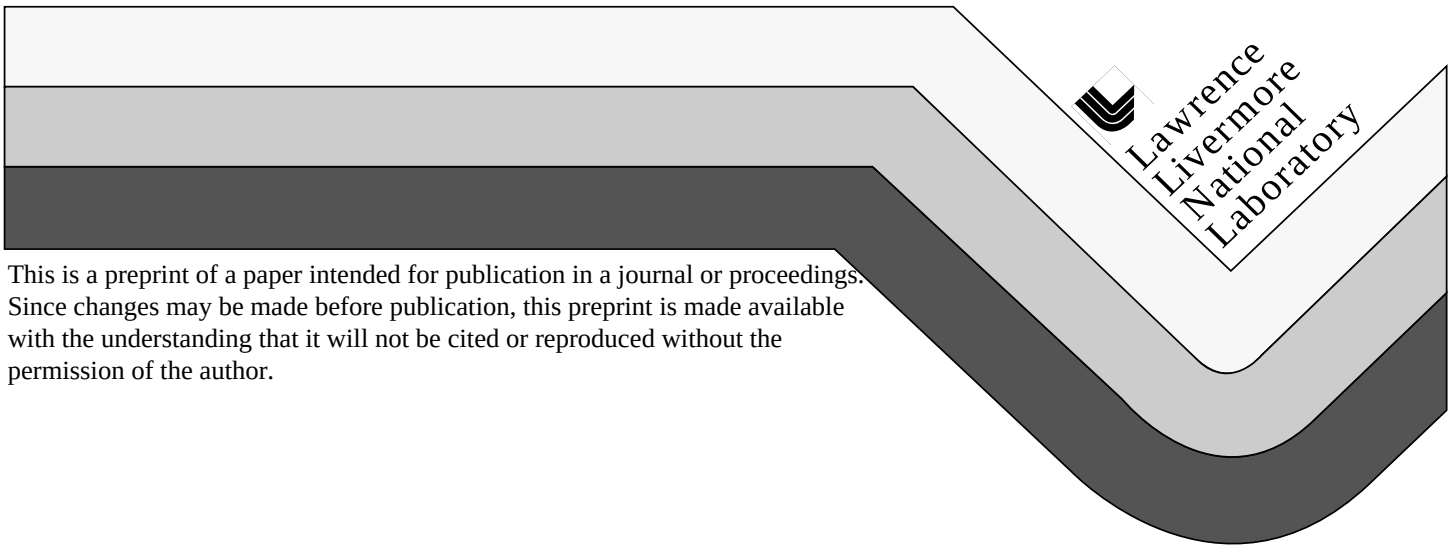

ELASTIC CONSTANTS OF β-HMX AND TANTALUM, EQUATIONS OF STATE OF SUPERCRITICAL FLUIDS AND FLUID MIXTURES AND THERMAL TRANSPORT DETERMINATIONS*

Joseph. M. Zaug
Lawrence Livermore National Laboratory, University of California,
P.O. Box 808, L-282, Livermore, California 94551

Ultrasonic sound speed measurements via Impulsive Stimulated Light Scattering (ISLS) were made in single crystals of β-HMX and tantalum over an extended range of temperatures. Elastic constants are consequently determined for β-HMX. Sound speeds are calculated for tantalum, from known elastic constants, and compare favorably with the results presented here. ISLS time-domain fits of tantalum records allowed for thermal diffusion determinations and, correspondingly, thermal conductivity. Measurements of the speed of sound and of the thermal diffusivities of fluid oxygen up to pressures of 13 GPa and at several temperatures are presented. Between 0.1 and 13 GPa the fluid's density increases by a factor of three. Thermal diffusivities rise slowly over this range, and are substantially smaller than those previously measured for the solid β-phase. Additional sound speed measurements were made along the 250° C isotherm in a 1:1 molar ratio mixture of liquid oxygen and nitrogen. These experiments demonstrate the versatility and potential application of a new laboratory within the U. S. DOD and DOE complex.[1]

I. INTRODUCTION

Experiments at very high pressures provide insight into a realm of chemical and material properties that are significantly different from those encountered under ambient conditions. Such studies extend and test the theoretical framework which permits progress from properties at the atomic and molecular level to macroscopic behavior, constitute a potential source of novel materials and new tools for chemical transformation and are important adjuncts to progress in other disciplines. There is no question that an improved general knowledge of electronic, physical, and chemical behavior of relevant constituent materials at high density is required, for example, for a less fragmented description of the processes that precede and direct exothermic chemical reactions. The same arguments are routinely made with regard to the structure and evolution of the major planets[2] and the deep interior of the Earth.

Dynamical simulation based on approximate Born-Oppenheimer potentials plays a large and increasingly important role in chemistry and in the biological and materials sciences. More generally, knowledge of an effective interatomic potential function underlies any effort to predict or rationalize the properties of solids and liquids. Particularly in systems associated with experimentally difficult temperatures or pressures, such as prevail in the deep interiors of the Earth and giant planets, dynamical simulation based on computed potentials seems at present the most promising predictive resource. While there exists an extensive body of experimental techniques and experience on computational methods appropriate to ambient conditions, the regime of strong repulsive interactions at very high densities has not been as extensively investigated.[3-10] The experiments discussed here are aimed both at enlarging the family of properties conveniently measured at high pressure and, principally, at providing the data appropriate to a critical test of the theory of the internuclear potential in simple substances at high density.

II. ELASTIC CONSTANTS AND THERMAL DIFFUSIVITY AS GUIDES TO THEORY

A. ELASTIC CONSTANTS

Crystallographic investigation of the high pressure equation of state of solids has been the principal experimental probe into interatomic and intermolecular forces in condensed phases in the region of strong repulsive interactions. Two-body central-force potentials, on occasion augmented by the Axilrod-Teller three-body interaction,[11] have successfully reproduced the equation of state of a number of highly symmetrical solids. However, theoretical estimates[8,9] of three-body exchange interactions predict a significant deviation from purely pair repulsive potentials even at distances corresponding to moderate pressures. It has been argued[8] that the

*This work was supported by the auspices of the U.S Department of Energy at Lawrence Livermore National Laboratory under contract number W-7405-Eng-48.

many-body exchange interaction, however essential it may be to an adequate general description of systems at high density, plays a relatively small role in those deformations that preserve the high site symmetry of simple crystal structures, and so minimize the distortion of atomic or molecular wave functions. It then follows that an approach to the interaction energy that reproduces the pressure-density relation of a crystal cannot be transferred with confidence to less symmetrical situations.

In contrast to hydrostatic pressure, long-wave acoustic phonons alter the local crystal symmetry, thus the prediction of their velocities (parameterized in the elastic constants) constitutes a more searching test of an empirical potential or computational approach. A good example of this difference is seen in the Decker model of NaCl. This model has been so successful in reproducing the experimental equation of state that it has been recommended for use as a pressure standard.[12,13] However, the central pair potential on which it is based is intrinsically incapable of reproducing the large deviations from the Cauchy relations[14] exhibited by the elastic constants.[15] In consequence, it may be assumed that the model will also fail to reproduce the phonon dispersion relations and the thermodynamic and transport properties of the crystal.

In the general attempt to define a useful potential, a complete set of elastic constants of a highly compressible crystal, determined over a considerable range of nearest-neighbor distances, provides an optimal basis for the confrontation of computational approaches with experiment.

B. THERMAL DIFFUSIVITY

The theory of thermal transport in insulators, and its pressure dependence, has ranged from calculations based on fairly realistic microscopic models[16,17] to qualitative rationalizations based on the Debye-Grüneisen model.[18-20] Within the context of the latter, a knowledge of the volume dependence of force constants (derived from the pressure dependence of the elastic constants) permits the calculation of the individual mode Grüneisen parameters of a lattice-dynamical model, and thus an evaluation of the pressure dependence and anisotropy of the thermal diffusivity. This may then be compared with the experimentally derived quantities.

The extension of either microscopic or phenomenological theory to extreme conditions requires data on at least a few simple systems over an extended range of densities. In conjunction with a theory based on interatomic potentials, the experimental determination of thermal transport provides another manner of proving computational progress.

III. EXPERIMENTAL TECHNIQUE

A. SAMPLE PREPARATIONS

1. β-HMX

Single crystals of β-HMX (~5 mm long x ~2 mm thick) were mounted with beeswax on a glass carrier substrate and coarsely ground using 1 μm alumina slurry on either silk (better) or non-woven textile ("Texmet", less well) cloths. This combination of coarse abrasive and hard-surface cloth is selected to flatten the gross plane of polish parallel to the glued-down, rear reference face of the crystal. At the conclusion of 1μm polishing, a substantial pit density remains. Similar fine grinding on hard cloth with 0.3 μm alumina eliminates the pit density readily, again with surprising removal rate and good surface flatness. A brief final polish on a relatively hard cloth ("OP-chem") using a colloidal silica dramatically improves the quality of the surface. Care must be taken to rinse the silica buildup out of the colloid. This final stage tends to round edges significantly and can't be carried out more than about 30 seconds. The application of heat (< 100° C) easily removed samples from the substrate. Isopropanol was used to remove the wax. To prevent chemical etching of samples exposure to isopropanol was kept to a minimum.

2. SUPERCRITICAL O_2 AND N_2-O_2

Merrill-Bassett type Diamond anvil cells (DAC's) were loaded with 99.999% fluid oxygen and 99.9% 1:1 molar mixture of nitrogen + oxygen at one atmosphere, sealed and subsequently brought to high pressure. It was found in previous work on supercritical water at high temperature that gold could be used to prevent oxidation of the gasket. In addition, the high reflectivity of the gold measurably reduces the propensity of soot formation when the pulsed excitation beams clip the gasket. Gold-lined 316 stainless steel and Inconel® X-750 gaskets were used to laterally confine the supercritical fluids. Producing gold lined rhenium gaskets was extremely difficult. The gold would fill into open rhenium cracks and reduce the friction required to lock a gasket around a confined sample. For high temperature work, the DAC sat inside a resistively heated vacuum oven. The temperature gradient around the DAC frame at 500° C was 8° C. The gradient within the sample region would be considerably less.

3. TANTALUM

The primary challenge in polishing very thin samples of tantalum is the difficulty in affixing the parts to a carrier substrate. Under load the samples will disbond from the fixative. A number of waxes and glues were experimented with before settling on "Crystal Bond®" by Universal. The samples were waxed onto a 35 mm diameter glass plate 10 mm thick. Grinding was done by hand, using 30 μm aluminum oxide for heavy stock removal, then 9 μm aluminum oxide to prepare the surface for fine polishing. Polishing was done on a "73 Gugolz" pitch lap using "Nalco® 2360" colloidal silica. Soaking the parts in acetone dissolved the

Crystal Bond,® allowing the parts to be removed without additional stress.

B. DETERMINATION OF VELOCITIES AND THERMAL DIFFUSIVITIES

The optical technique is discussed in general in Refs (21-22) and specifically in the context of the DAC in Refs. (23-25). Briefly, two successive "excitation" pulses, (30 μJ, 60 μm diameter, 100 ps duration) are selected from the output train of a Q-switched (500 Hz), mode-locked Nd:YAG laser and recombined in the sample at an angle 2θ, but otherwise coincident in space and time. Interference establishes a periodic distribution of intensity and, in a sample that absorbs in the near infrared, a (spatially) periodic variation in the temperature and pressure ensues. The coupling between laser light and the excited material modes is such that the local temperature rise remains "impulsive." The associated thermal pressure launches counter-propagating acoustic waves. The acoustic wavelength, d, in this case equal to the period of the optical grating, may be expressed in terms of the excitation wavelength, λ_E =1.064μm, and θ as

$$d = \lambda_A = \frac{\lambda_E}{2\sin\theta} \qquad (1)$$

In an arbitrary crystallographic direction in an elastically anisotropic crystal, one quasi-longitudinal and two quasi-transverse waves are excited. The impulsively excited acoustic waves induce a temporally and spatially periodic variation in the index of refraction of the sample. A third pulse (5 μJ, 20 μm diameter, 80 ps duration) selected from the same Q-switched envelope as the excitation pulses is frequency doubled (λ_p = 0.532 μm) and delayed by a combination of time of flight and mode lock pulse selection to generate the "probe." Observation of the intensity of the Bragg scattering of the probe, by the acoustic or thermoacoustic grating, as a function of probe delay serves to determine the frequency (ν), and hence the adiabatic velocity (c = dν) of the acoustic waves.

In practice, grating spacings are determined by making the same measurement on a piece of glass with a known speed of sound and which gives a strong, stable signal suitable for a calibrant. The glass was in turn calibrated against water and fused silica.[26-28] The velocity is typically determined with a precision of ±0.2%.

An example time-domain record for a single crystal of β-HMX is shown in Figure 1a. The quasi-longitudinal mode and one quasi-shear mode (most likely the more intense horizontal component) can be observed in the Fourier transform of this record (Figure 1b). If the samples(s) are rotated it is possible to measure velocities as a function of crystallographic direction (Figure 2) and hence deduce the individual elastic constants of the crystal. In the case where samples are not transparent in the near infrared, the bulk waves are probed using a cw argon$^+$ laser reflected off of the sample surface.

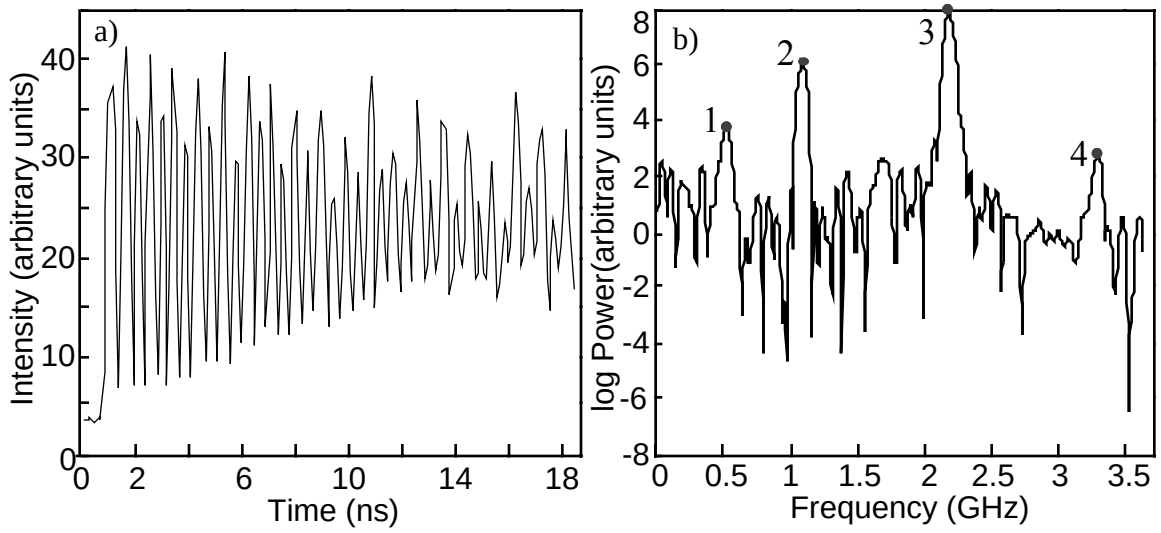

FIGURE 1. a) ISLS TIME-DOMAIN SPECTRA OF β-HMX AND b) CORRESPONDING POWER SPECTRUM AT 24.12°C. THE ACOUSTIC WAVELENGTH IS 1.55 μm. IN THE FREQUENCY-DOMAIN PLOT PEAK #1 IS REPRESENTATIVE OF THE THERMOACOUSTICLY COUPLED QUASI-SHEAR WAVE, PROBABLY HORIZONTALLY POLARIZED, PEAK #2 IS THE ELECTROSTRICTIVELY COUPLED QUASI-LONGITUDINAL WAVE, PEAK #3 IS THE THERMOACOUSTICLY COUPLED QUASI-LONGITUDINAL WAVE, AND PEAK #4 IS THE RESULT OF HARMONIC MIXING OR ADDITION OF PEAKS TWO AND THREE. IN THIS EXAMPLE THE QUASI-LONGITUDINAL VELOCITY, REGARDLESS OF THE OPTICAL COUPLING MECHANISM, IS 3.302 km/sec AND THE QUASI-SHEAR VELOCITY IS 1.595 km/sec.

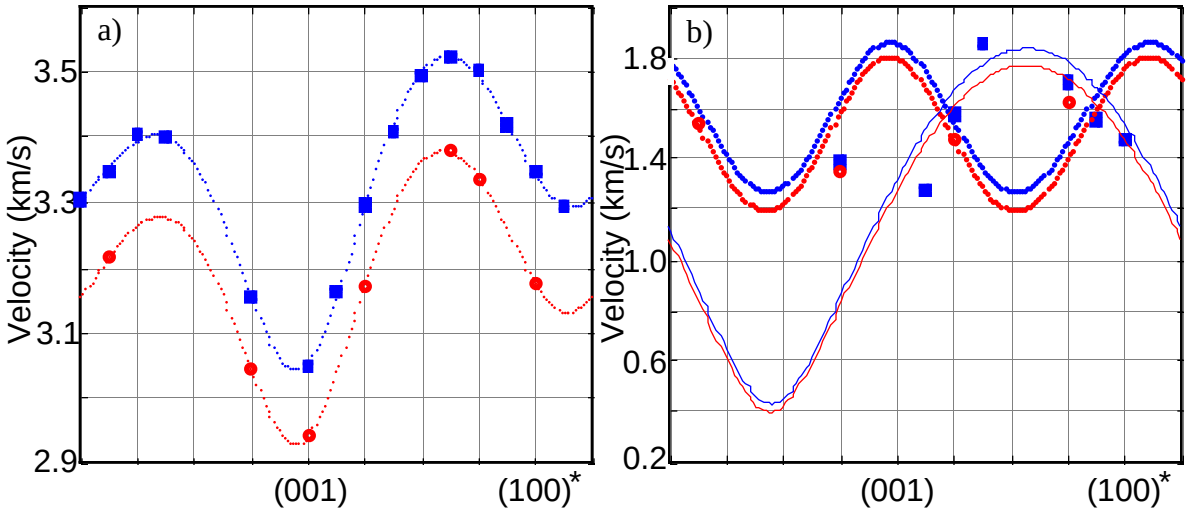

FIGURE 2. a) ISLS DATA SHOWING THE VARIATION IN THE SPEED OF SOUND AS THE ACOUSTIC WAVE VECTOR IS ROTATED WITHIN A (010) CRYSTAL OF β–HMX AT ROOM PRESSURE AND TWO DIFFERENT TEMPERATURES, 24° C FILLED SQUARES & 107° C FILLED CIRCLES. BOTH THE QUASI-LONGITUDINAL (FIGURE 2a) AND THE QUASI-TRANSVERSE (FIGURE 2b) BRANCHES ARE SHOWN. THE LINES ARE THE RESULT OF ADJUSTING THE THIRTEEN ELASTIC CONSTANTS TO FIT THE DATA. THE THICKER LINES IN 2b) REPRESENT THE HORIZONTALLY POLARIZED SHEAR WAVES WHILE THIN LINES REPRESENT THE VERTICALLY POLARIZED SHEAR WAVES.

In an absorbing medium, when the acoustic disturbance propagates beyond the area illuminated by the probe a spatially periodic distribution of temperature and hence index of refraction remains. This grating decays exponentially by thermal diffusion. The strength of the diffracted cw probe beam is recorded by an oscilloscope attached to a photomultiplier tube. The characteristic thermal decay time, τ_{th}, in a medium of density ρ, specific heat at constant pressure c_p, and thermal conductivity κ, is given by

$$\tau_{th} = \frac{\rho c_p d^2}{4\pi^2 \kappa} = \frac{d^2}{4\pi^2 D_{th}} \qquad (2)$$

with $D_{th}=\kappa/\rho c_p$ where D_{th} is the thermal diffusivity. The scattered intensity is proportional to the square of the amplitude, thus the signal decays as $\exp(-2t/\tau_{th})$. If d is sufficiently small so that conduction normal to the plane of the sample is unimportant a plot of the inverse relaxation time *versus* d^{-2} will be linear. On the time scale displayed in Figure 3a scattering by the thermal grating appears as a time-independent contribution to the intensity. Here the decay of the thermal grating at longer times is apparent where it is shown for several different values of the grating period. A plot of τ_{th}^{-1} versus d^{-2}, shown in Figure 3b, yields a straight line through the origin with slope equal to $8\pi^2 D_{th}$. Determination of the anisotropy of thermal diffusivity is a simple matter of rotating the crystal in order to produce the thermal grating along different directions.

C. DETERMINATION OF PRESSURES

Pressure determinations were made by monitoring the wavelength of the fluorescence (excited by a He-Cd laser or by the 488-nm Ar^+ laser line) of ruby chips which surround or are embedded in the sample. Rubies after grinding to tens of microns have residual strains which are often large enough to offset pressure measurements by ~0.05 GPa, and occasionally as much as 0.2 GPa. Annealing at ~1000° C for several hours decreases both the magnitude and frequency of these deviations yet it is still common to find rubies which differ reproducibly by the equivalent of 0.02 GPa. The most precise work completed has been on the melting curve of O_2, in which the relative wavelengths of rubies were recorded at 0 GPa and the high-pressure results corrected by the same amounts. The reference rubies at 0 GPa were kept in the same temperature controlled housing as were the samples, because wavelength shifts equivalent to 0.01 GPa are generated by temperature differences of 0.5° C and in order to match as closely as possible the two spectral line shapes. With hydrostatic samples one can measure pressures with a precision of slightly better than 0.01 GPa. A dispersion of 4.08×10^{-3} Å/bin resulted from the combination of a 750 bin CCD camera and a 1/4 m monochromator. (1200 grooves/mm grating.)

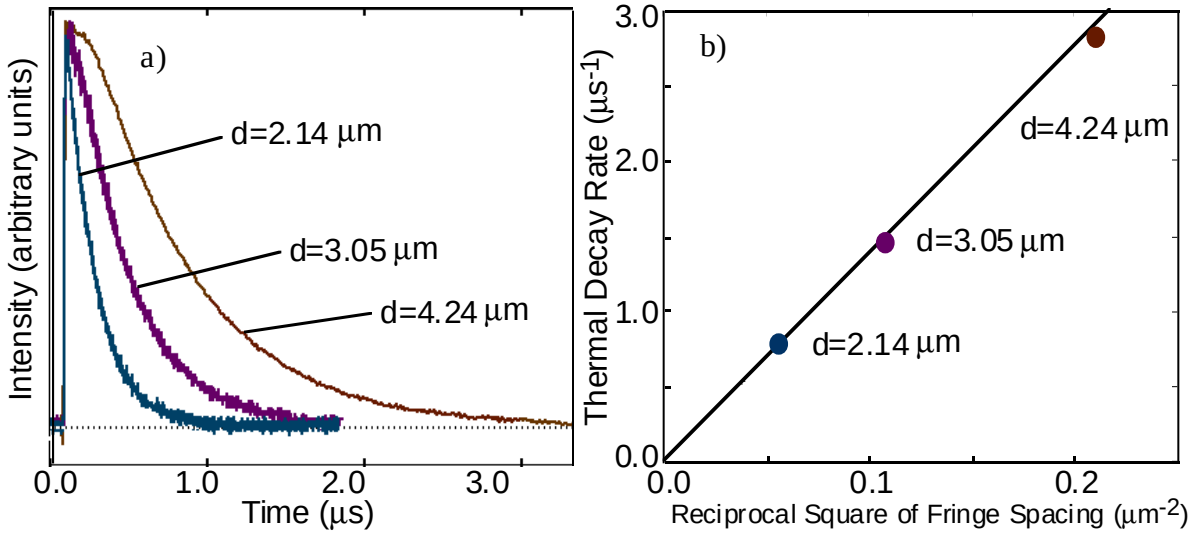

FIGURE 3. a) β-OXYGEN AT 6.40 GPa and 29° C.[43] THE THERMAL GRATING DECAYS EXPONENTIALLY WITH TIME-CONSTANT PROPORTIONAL TO THE SQUARE OF THE GRATING PERIOD, d. TRACES ARE SHOWN FOR GRATINGS OF PERIOD 4.24, 3.05, AND 2.14 μm. b) THE INVERSE TIME-CONSTANT PLOTTED AGAINST THE INVERSE SQUARE OF THE GRATING PERIOD FOR THE DATA SHOWN IN FIGURE 3a. THE STRAIGHT LINE PASSING THROUGH THE ORIGIN IS INDICATIVE OF ONE-DIMENSIONAL HEAT FLOW; THE MEASURED THERMAL DIFFUSIVITY IS 3.49X10^{-7}m^2/s.

D. DETERMINATION OF CRYSTAL ORIENTATIONS

Two β-HMX crystals were x-ray oriented on an Enraf-Nonius CAD4 diffractometer at room temperature. Graphite monochromatized, Mo-Kα radiation was used. The power was set to 50 kV and 26 mA. Crystals were aligned so that the beam was always contained within the sample. The direct orientation matrix was determined from 12 Bragg reflections, with 2θ ranging from 8 degrees to 25 degrees. The cell was checked against literature values and was found to agree within experimental error. Each crystal alignment was completed in about 4 hours. The normalized direct orientation matrix (crystallographic axis magnitudes along the laboratory x, y, and z coordinates) and the plane normal to the axis of rotation corresponding to the data plotted in Figure 2 are provided in Table 1. Sound speed measurements were made by rotating samples about the laboratory x-axis. The approximate (001) orientation of a single crystal of tantalum was made by x-ray precession photography.

TABLE 1. NORMALIZED ORIENTATION MATRIX AND PLANE NORMAL TO AXIS OF ROTATION

	x	y	z
a	-0.025608	0.98949	0.14230
b	0.99934	0.029686	0.020789
c	0.01858	-0.07771	-0.9968

a	**b**	**c**
2.7973e-02	9.9934e-01	2.3037e-02

IV. EXPERIMENTAL RESULTS & DISCUSSION

A. DETERMINATION OF ELASTIC CONSTANTS FROM MEASURED VELOCITIES

1. β-HMX

For monoclinic crystals with symmetry axis **b**, the 13 elastic constants are defined with reference to three orthogonal axes $\mathbf{i}_3$, $\mathbf{i}_2$, $\mathbf{i}_1$, where $\mathbf{i}_3$ correspond to the **c**-axis, the respective **b**-axis, and their mutually perpendicular axis, **a***-axis. The velocity V of an acoustic wave with direction cosines y_i in a crystal of density ρ is given by[29]

$$\left|A_{ij} - \rho V^2 \mathbf{I}\right| = 0, \tag{2}$$

where **I** is the identity matrix, and A is

$$\begin{aligned}
A_{11} &= y_1^2 c_{11} + y_2^2 c_{66} + y_3^2 c_{55} + 2y_1 y_3 c_{15},\\
A_{22} &= y_1^2 c_{66} + y_2^2 c_{22} + y_3^2 c_{44} + 2y_1 y_3 c_{46},\\
A_{33} &= y_1^2 c_{55} + y_2^2 c_{44} + y_3^2 c_{33} + 2y_1 y_3 c_{35},\\
A_{12} &= y_2 y_3 (c_{46} + c_{25}) + y_1 y_2 (c_{12} + c_{66}),\\
A_{13} &= y_1^2 c_{15} + y_2^2 c_{46} + y_3^2 c_{35} + y_1 y_3 (c_{13} + c_{55}),\\
A_{23} &= y_2 y_3 (c_{44} + c_{23}) + y_1 y_2 (c_{25} + c_{46}).
\end{aligned} \tag{3}$$

Along certain symmetry directions, or for crystals of high symmetry, Eq. 3 factors such that the velocity of an acoustic wave is dependent on only one elastic constant, and thus a single velocity measurement constrains a specific elastic constant.[30] However, in the case of monoclinic materials, the number of such directions is restricted. For propagation along the **b**-axis (that is, y_1=0, y_2=1, y_3=0), the equation reduces to

$$\left(c_{22} - \rho V^2\right)\left[\left(c_{44} - \rho V^2\right)\left(c_{66} - \rho V^2\right) - c_{46}^2\right] = 0 \tag{4}$$

which yields a compressional velocity $V^2 = c_{22}/\rho$ and a quadratic in three elastic constants whose roots are the two shear velocities. For propagation in the **a**-direction, c_{66} is similarly determined from a single shear velocity and for propagation in the **c**-direction, c_{44} is the sole elastic constant that determines the velocity of a shear wave. In all other propagation directions, velocities are determined by a minimum of three, though usually more, elastic constants, in various combinations.

An iterative, non-linear, least-squares simplex algorithm[31] was used to find the set of elastic constants that optimally fits measured compressional velocities. Initial room temperature fits were weighted to an experimentally determined bulk modulus of 12.50 GPa. The high temperature density was calculated using a volume expansion value of 162.5 μm/m/K for which ΔT=83° C. With only two samples available, of similar orientations, the number of elastic constants that contribute to the observed sound speeds is limited (i.e., c_{11}, c_{15}, c_{33}, c_{35}, and c_{55}). For similar reasons the shear speeds were not fit. However, there is a tendency for agreement. (see Figure 2b.) Velocity residuals, based on this fit, follow an approximately normal distribution with a root-mean-square misfit of 7 ±1 m/s. The resulting elastic constants and their 2σ (95% confidence) uncertainties are summarized in Table 2. The misfit does not represent a unique and global minima. Obtaining data within two additional crystal orientations would serve to over-determine the elastic constant values.

TABLE 2. ELASTIC CONSTANTS IN UNITS OF GPa. ARROWS POINT TO THE 107° C FIT RESULTS. *K* AND *G* ARE THE RESPECTIVE ADIABATIC AGGREGATE BULK AND SHEAR MODULUS (VOIGT UPPER LIMITS).

C_{11}	20.8→18.7 (0.3)	**C_{35}**	0.1 → 0.1 (0.1)
C_{12}	4.0 → 3.8	**C_{44}**	2.9 → 2.7
C_{13}	13.0→ 12.0	**C_{46}**	3.0 → 2.9
C_{15}	0.6 → 0.4 (0.1)	**C_{55}**	6.6 → 6.1 (0.2)
C_{22}	26.9→ 25.8	**C_{66}**	3.8 → 3.5
C_{23}	6.6 → 6.5	*K*	12.51→ 11.67
C_{25}	-1.5 → -1.4	*G*	5.43 → 5.00
C_{33}	17.6→16.1 (0.2)	density (g/cc)	1.903 →1.877

2. TANTALUM

At ambient pressure, in metals or other materials which are not transparent in the near infrared, parallel-polarized pulses will excite not bulk acoustic waves but Rayleigh waves, and very strong coherent scattering from the surface corrugation is observed.[32] The time domain records of tantalum indicate that the relaxation time of the thermal grating is less than the time required for the damping of the acoustic wave. The following form[32], $I=(A_{th}e^{-t/\tau} - A_{ac}e^{-\gamma t}\cos\omega t)^2$, gives a good account of the scattered intensity, I as a function of probe delay t. Here A_{th} is the amplitude of the thermal grating, A_{ac} is the amplitude of the acoustic grating, ω the circular acoustic frequency ($\omega=2\pi f$), and γ the temporal acoustic absorption coefficient. The thermal and acoustic parameters are determined by making least-squares parameter adjustments to fit ISLS time-domain records. Care has been taken to account for the effects of geometric runout of the probe beam. The thermal decay time, determined from ISLS records, in tantalum at 26° C increased by 5.5% to 9.0 ns at 396° C. The acoustic wavelength was 1.52 µm. The corresponding thermal diffusivity changed from 2.49 x 10^{-4} to 2.63 x 10^{-4} m^2/s, and using literature data for the density and specific heat at constant pressure it is determined that the thermal conductivity changes from 58.9 to 63.3 ±1.4 W/m/K.

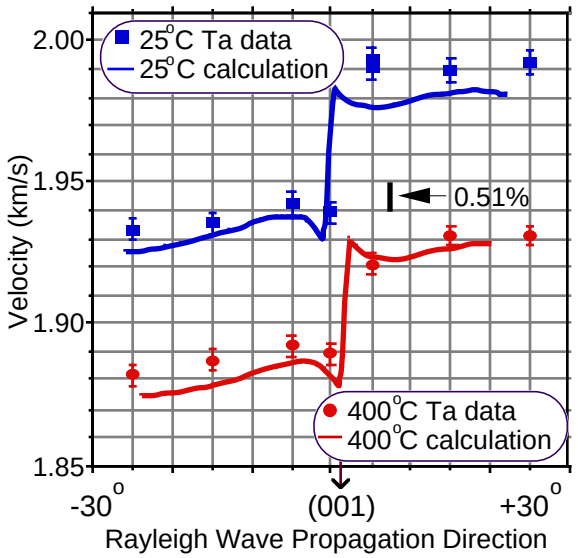

FIGURE 4. ISLS SURFACE WAVE DATA, ON A SINGLE CRYSTAL OF Ta, SHOWING THE VELOCITY DEPENDENCE ON CRYSTALLOGRAPHIC DIRECTION AND TEMPERATURE. THE SOLID LINES REPRESENT CALCULATIONS BASED ON PREVIOUSLY PUBLISHED ELASTIC CONSTANT DATA.

In Figure 4, the temperature and orientational dependence of the surface acoustic wave velocities on a approximately (100) tantalum crystal are plotted. The c_{44} elastic constant is known up to 2,727° C.[33] The c_{11} and c_{22} constants and density of tantalum are known up to 500° C.[34] This data was used to calculate surface wave velocities given an exact (100) sample orientation. The work presented here simply demonstrates the utility of the technique and the opportunity to produce more accurate determinations of both elastic constants and equations of state of opaque materials. Electrical heating of tantalum will permit optical determinations of the three elastic constants up to the melting point, 3,017° C. Determining the EOS using DAC's is currently underway. ISLS can also be utilized to study higher symmetry materials (*i.e.*, Pu) for which more traditional techniques, such as resonant ultrasound spectroscopy, produce ambiguous results.[35]

B. DETERMINATION OF EQUATIONS OF STATE FROM MEASURED VELOCITIES

Measurements of the speed of sound in supercritical oxygen have been made along two isotherms of 30° and

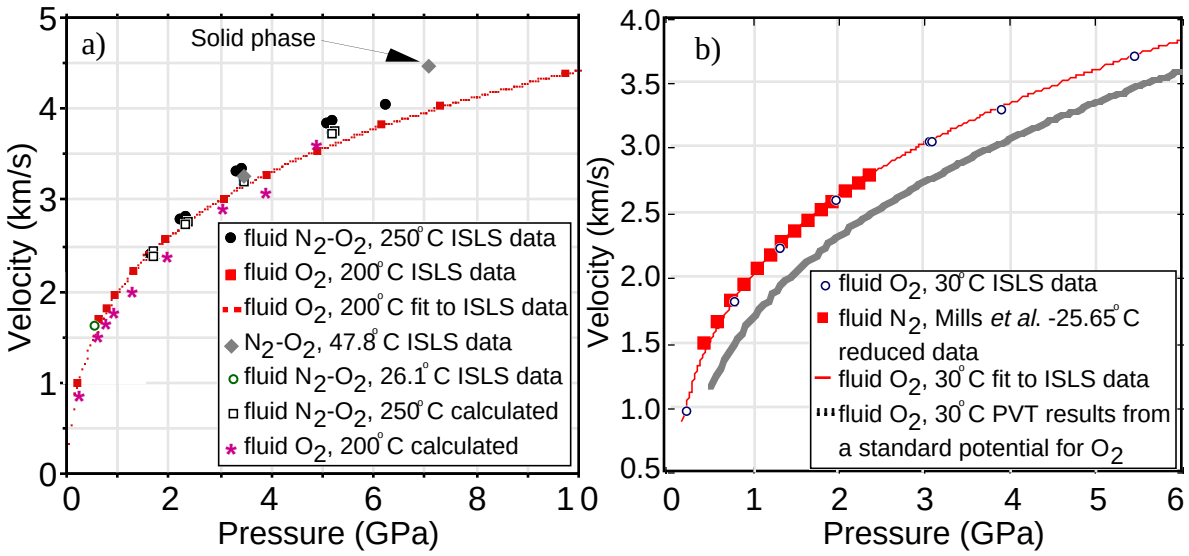

FIGURE 5. a) ISLS SOUND SPEED DATA AND CORRESPONDING CALCULATIONS FOR OXYGEN AND 1:1 MOLAR RATIO OF FLUID OXYGEN TO NITROGEN. b) EXAMPLE OF THE LAW OF CORRESPONDING STATES FOR O_2 AND N_2. THE N_2 DATA[40] ARE REDUCED BY THE CRITICAL PRESSURE, TEMPERATURE AND DENSITY AND COMPARED AGAINST THE ISLS O_2 DATA AT 30° C. THE DASHED LINE IS A MOLECULAR DYNAMIC RESULT USING A STANDARD POTENTIAL.[38] FOR O_2 A C_P AT LOW PRESSURE, WHERE REASONABLY KNOWN, WAS USED TO START THE INTEGRATION NECESSARY TO GENERATE THE SOUND SPEEDS.

200° C, and in a 1:1 molar mixture of N_2 + O_2 along a 250° C isotherm. (see Figure 5a.) Each oxygen isotherm was followed up to near the freezing points (5.9 and 12GPa). Starting with known values of density, ρ, and specific heat, C_P, the thermodynamic equation of state is calculated by recursive numerical integration of

$$\left(\frac{\partial \rho}{\partial P}\right)_T = (c_o)^{-2} + \left(\frac{\alpha^2 T}{C_P}\right) \text{ and } \left(\frac{\partial C_P}{\partial P}\right)_T = \left(\frac{\partial^2 V}{\partial T^2}\right)_P \quad (5)$$

where P, c_o, α, T, and V are respectively the pressure, zero frequency sound speed, thermal expansion coefficient, absolute temperature, and specific volume. In this work, initial values of ρ and C_P were taken from the EOS of Wagner *et al*.[36]

An overview of previous work on oxygen is given by Wagner and Schmidt (W&S).[36] These authors have generated a thermodynamic potential based on experimental densities up to 0.08 GPa and at 130° C up to 0.03 GPa. In addition, they used combined density and heat capacities measured to 30° C and 0.03 GPa. Other data, not used by Wagner and Schmidt, are those of Tsiklis and Kulikova,[37] who measured densities to 1 GPa and 400°C. The latter were used above 0.2 GPa by Belonoshko and Saxena (B&S)[38] to constrain a molecular dynamics simulation (based on an exponential-6 potential) which was in turn used to construct a P-V-T surface. A Shock Hugoniot for the 1:1 fluid mixture provides P-V-E data between 9.89 and 24.0GPa.[39]

The data presented here are currently insufficient to make a "positive" determination of the equation of state of O_2 or the mixture. The high-pressure sound speed data, especially at higher temperatures, do not extend to the lower pressures at which values for C_p and ρ, are known. Further, the small variations in speed of sound concomitant, with the experimentally useful range of temperatures used here are small enough to be confounded with the uncertainties in the measurements of pressure. Consequently, several approximations have been made to yield a reasonably accurate EOS. The results are then compared with other data.

The assumptions made are that the sound speeds are linear in T over the stated range, that the W&S EOS correctly predicts the speeds up to 0.5 GPa, and that the form of the interpolating function is suitable to the task. At pressures higher than 0.7GPa the speeds are assumed to vary linearly between 30 and 200° C, and an artificial data set is calculated at 6 temperatures from 30° C to 100° C, based on the previous fits at the two stated end temperatures. Each isotherm is then fit individually, with the fits forced to conform to the W&S EOS for pressures between 0.02 and 0.05 GPa. The result is a velocity field in P and T in which the velocities are linear interpolations in T above 0.7GPa, fairing into the W&S EOS below that. The usual equations are then iteratively solved to obtain the densities, heat capacities, entropies, etc. The results are reasonable, the densities increasing monotonically while remaining below those of the β phase. The heat capacities, C_P are fairly constant in pressure, varying by at most 5% for each isotherm. They undergo several oscillations with increasing pressure which probably derive from the cross-over of dc/dT from a positive to a negative value at 0.5 g/cm^3.

At 30° C the O_2 densities determined here are 8% higher than the B&S results up to 0.5GPa, then cross at

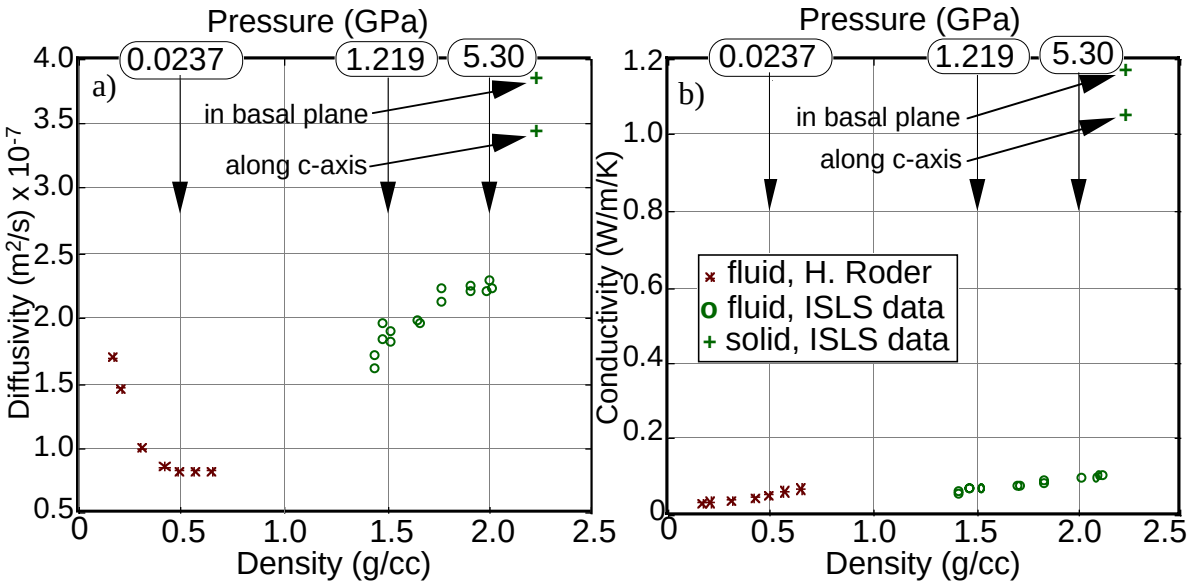

FIGURE 6. a) THERMAL DIFFUSIVITY OF OXYGEN AND b) CORRESPONDING THERMAL CONDUCTIVITY AT 30° C. CROSSES REPRESENT β-OXYGEN DATA AT 6.13 GPa AND 29° C. THE STATED PRESSURES CORRESPOND TO THE FLUID.

about 1.5 GPa and are then uniformly lower than B&S, by 10% at 6GPa. B&S densities are, however, always less than that of the solid, β phase. Given reasonable values of C_P (at 0.5 GPa), either from W&S results or those determined here, the speeds of sound inferred from the B&S EOS are uniformly low by about 10% (see Figure 5b). In comparison, this discrepancy is due to their higher compressibilities below ~4 GPa and higher densities above 2 GPa. In order to make their speeds of sound agree (approximately) with results here at 30° C it is necessary to assume an initial C_P at 0.5GPa of 9.2 J/K/mole at 30° C which is about 5 times lower than expected.

Speeds of sound were measured at 30° C and 1.5 GPa at frequencies of 1.3, 0.77 and 0.27 GHz. Velocities matched to within the uncertainties, *i.e.* ±0.2% for the higher frequency and ±0.5% for the two lowest. The ISLS velocities fair nicely into those of the W&S model and are lower than the extrapolation of W&S. More dispersion may exist at lower frequencies.

Between 22° C and 122° C the fluid β-phase boundary is well fit by the straight line P(GPa) = 0.0270 T(° C) + 5.153 with a two σ uncertainty on the slope of 10^{-4} GPa/° C. Each point of equilibrium was established by a visual observation of the simultaneous presence of both phases. Among observations, the volume of solid varied from approximately 5 to 95% of the sample; no correlation was apparent between the deviations of the data from the fit and the fraction of solid. Since one expects that any impurities will be concentrated in the fluid, this fact suggests strongly that impurities had no significant effect on the measurements.

The measured oxygen velocities fit well to the form $\Sigma A_i \ln P^i$ with i={0...4}. The 30° → 200° C fit parameters are A_0=2.0438→1.8665, A_1=0.7764→0.8462, A_2=0.1040→0.140, A_3=0.0078 → -0.0020, and A_4=0.0010 → -0.0016. In such fits the data were supplemented by points at lower pressures generated from the W&S EOS. Additionally, the curve at 30° C was constrained to lie along the 200° C isotherm above 7 GPa. N_2-O_2 fit parameters from 1.3 to 6.5 GPa at 250° C are A_0=2.0058, A_1=0.4490, A_2=0.8424, A_3= -0.2605, and A_4= -0.0015. A 1:1 molar ratio of N_2-O_2 at 25° C forms δ-N_2 at approximately 4.3 GPa[41] which accounts for the significant increase in velocity observed at 7.1 GPa. The calculated points in Figure 5a were derived from an accurate EOS for exp-6 type fluids[42] based on HSMA integral equation theory and Monte Carlo calculations.

According to simple theories, substances should behave the same when all variables are suitably scaled and the critical parameters are the most common scaling factors chosen. Figure 5b shows Mills et al. –25.5° C data, which is equivalent to oxygen at 30° C when scaling by the critical temperatures. The N_2 sound speeds are reduced using critical pressures and densities.

$$c_{O_2}(\text{equivlent}) = c_{N_2} * \frac{\sqrt{\frac{P_c(O_2)}{P_c(N_2)}}}{\sqrt{\frac{Mw(O_2)}{Mw(N_2)}} * \sqrt{\frac{\rho_c(O_2)}{\rho_c(N_2)}}} \qquad (6)$$

Since O_2 and N_2 have the exact same compressibility factor ($P_cV_c/RT_c = 0.292$), and the no dipole moment, it may not be too much of a surprise that the sound speeds correlate well with the empirical law of corresponding states. This result suggests that N_2 and O_2 molecules are approximately spherical up to 2.2GPa.

C. DETERMINATION OF THERMAL TRANSPORT PROPERTIES

Thermal diffusion measurements were made in supercritical oxygen (Figure 6a) up to 10 GPa and converted to thermal conductivity (Figure 6b) using C_P's derived by extending the W&S EOS to ISLS integrated sound speeds along the 30° C isotherm. When plotted against density the diffusivity is seen to have a minimum near 0.5 g/cm^3. This seems to mark a changeover from the behavior of a gas, where the diffusivity decreases with pressure, to that of a liquid. Interestingly, 0.5 g/cm^3 is where the sound speed derivative changes from a positive (as in a saturated gas) to a negative value. The low density data appears to slightly overpredict the ISLS results. Measurements of α, C_P and ρ at higher pressures would perhaps help to resolve the difference.

V. SUMMARY

This paper represents a sample of continuing work on materials of immediate interest to the detonation physics community. Direct determination of the thermodynamic EOS (P,V,T) from measured temperatures, pressures and very accurate sound speeds, especially on supercritical fluid mixtures, will have a significant and positive impact on our ability to scientifically predict detonation energetics. The necessity for accurate density measurements, on relevant materials at higher pressures and temperatures, creates the opportunitiy for future collaborations. Isothermal compliance requires knowledge of $C_P(P,T)$.

VI. ACKNOWLEDGMENTS

Jerry Dick (LANL) provided HMX samples made by Howard Cady. The HMX x-ray orientation work was performed by Brian Scott (LANL), HMX polishing was partially done by Dave Phillips (LANL), tantalum polishing was completed by James Embree (LLNL), measurements on O_2 were taken by Dr. Evan Abramson and Mike Harrell (in collaboration with the Univ. of WA.) Mike Howard (LLNL) ran exp-6 calculations. The author also thanks LANL for the use of a high-temperature DAC oven. My aunt Dwan Oliver deserves many thanks for her warm hospitality during my exhausting sojourns in Seattle WA.

VII. REFERENCES & FOOTNOTES

1. The experiments discussed here were performed in collaboration with the University of Washington group (E. Abramson, M. Brown, M. Harrell, and L. Slutsky) while construction of a new and vastly improved system was being constructed at LLNL. The Livermore laboratory will be fully operational in October of 1998.

2. Stevenson, D. J., "The Interiors of the Giant Planets," *Ann. Rev. Earth Planet. Sci*., **10**, p. 257 (1982).

3. Cohen, A. J. and Gordon R.G., "Modified Electron Gas Study of the Stability, Elastic Properties and High Pressure Behavior of MgO and CaO Crystals," *Phys. Rev. B* **14**, p. 4593 (1976).

4. Waldman, M. and Gordon R.G., "Scaled Electron Gas Approximation for Intermolecular Forces," *J. Chem. Phys*., **71**, p. 1325, (1979).

5. LeSar, R. and Gordon R. G., "Density-Functional Theory for Solid Nitrogen and Carbon Dioxide at High Pressure," *J. Chem. Phys*., **78**, pp. 4991-4996, (1983).

6. Aziz, R.A., "Interatomic Potentials for Rare Gases: Pure and Mixed Interactions" in The Rare Gases, M. L. Klein, Ed. (Springer, New York, 1984).

7. Parinello, M. and Carr R., "Uniform Approach for Molecular Dynamics and Density-Functional Theory," *Phys. Rev. Lett*., **55**, p. 2471, (1985).

8. Barker, J. A., "Empirical Potential Functions for Rare Gases: Pair Potentials" in Simple Molecular Systems at Very High Density, A. Polian, P. Loubeyre, and N. Boccara, Eds., pp. 331-339, NATO ASI Series B: Physics **186** (Plenum Press, NY, 1989) , "Empirical Potential Functions for Rare Gases: Many-Body Potentials", *ibid*, pp. 341-351.

9. Bulski, M., "*Ab Initio* Pair and Three body Potentials" in Simple Molecular Systems at Very High Density, A. Polian, P. Loubeyre, and N. Boccara, Eds. pp. 331-339, NATO ASI Series B: Physics **186** (Plenum Press, NY, 1989).

10. Stoneham, A. M. and Harding J .H., "Interatomic Potentials in Solid State Physical Chemistry," *Annu. Rev. Phys. Chem.*, **37**, p. 53 (1986).

11. Axilrod, B. M. and Teller E., "Interaction of the van der Waals Type Between Three Atoms," *J. Chem. Phys*. **11**, p. 299, (1951).

12. Decker, D. C., "High-Pressure Equation of State for NaCl, KCl and CsCl," *J. Appl. Phys*., **42**, pp. 3239-3244, (1971)

13. Decker, D. L., Basset W. A., Merrill L., Hall H. T. and Barnett J. D., "High Pressure Calibration: A Critical Review," *J. Phys. Chem. Ref. Data*, **1**, pp. 773-835, (1972).

14. Born, M. and Huang K., Dynamical Theory of Crystal Lattices, (Oxford University, Oxford, 1954).

15. Kinoshita, H., Hamaya N., and Fujisawa H., "Elastic Properties of Single-Crystal NaCl under High Pressures to 80 Kbar," *J. Phys. Earth*, **27**, pp. 337-350, (1979).

16. Sindzingre, P. and Gillan M. J., "A Computer Simulation Study of Transport Coefficients in Alkali Halides," *J. Phys.: Condens. Matter*, **2**, pp. 7033-7042, (1990).

17. Pettersson, S., "Calculation of the Thermal Conductivity of Alkali Halide Crystals," *J. Phys. Chem*., **20**, pp. 1047-1061, (1987).

18 MacPherson, W. R. and Schloess H. H., "Apparent, Lattice and Radiative, Thermal Conductivity at Temperatures from 300 to 1500 K and Pressures up to 5.6GPa: Results for MgO and NaCl," *High Temperatures-High Pressures*, **15**, pp. 495-509, (1983).

19. White, G.K., "The Grüneisen Parameters and Pressure Dependence of Thermal Conductivity," *High Temperatures High Pressures*, **21**, pp. 233-236, (1989).

20. Gerlich, D. "Pressure Dependence of the Thermal Conductivity of Insulators," *J. Phys. Chem*., **15**, pp. 4305-4310, (1982).

21. Yan, Y. X., Cheng L. T., and Nelson K. A., "Impulsive Stimulated Scattering," in Advances in Non-linear Spectroscopy, J. H. Clark and R. E. Hester, Eds. John Wiley Ltd. London, (1987).

22. Fayer, M. D., "Holographic Grating Generation of Ultrasonic Waves," *IEEE J. Quantum Electronics*, **22**, p. 1444, (1986).

23. Brown, J. M., Slutsky L. J., Nelson K. A., and Cheng L. T., "Velocity of Sound and Equation of State of Methanol and Ethanol in a Diamond Anvil Cell: An Application of Impulsive Stimulated Scattering," *Science*, **241**, p. 65, (1988).

24. Zaug, J. M., Abramson, E. H., Brown, J. M. and Slutsky, L. J., "Elastic Constants, Equations of State and Thermal Diffusivity at High Pressure" in High Pressure Research; Applications to Earth and Planetary Sciences, Y. Syono and M. Manghnani Eds., pp. 157-166, American Geophysical Union, Washington D. C., (1992).

25. Zaug, J. M., Ph.D. Thesis, (University of Washington, Seattle, December 1994).

26. Greenspan, M., and Tschiegg, C. E, "Tables of the Speed of Sound in Water"., *J. Acoust. Soc. Am.*, **31**, pp. 75-76, (1959).

27. Wilson W. D., "Speed of Sound in Distilled Water as a Function of Temperature and Pressure," *J. Acoust. Soc. Am*., **31**, pp. 1067-1072, (1959).

28. American Institute of Physics Handbook (McGraw-Hill, New York, 1957).

29. Mason, W. P., Physical Acoustics and the Properties of Solids, (D. Van Nostrand, Princeton, N.J., 1958).

30. Abramson E. H., Brown J. M., Slutsky L. J., and Zaug J. M., "The Eleastic Constants of San Carlos olivine to 17 GPa," *J. Geophys. Res*., **B6-102**, 12253-12263, (1997).

31. Press W. H., Flannery B. P., Teukolsky S. A., and Wetterling W. T., "Downhill Simplex Method in Multidimensions" In: Numerical Recipes: The Art of Scientific Computing," (Cambridge University, New York, pp. 289-293, 1986).

32. Cheng, L. T., Ph.D. Thesis, (MIT, Cambridge, Massachusetts, June 1988).

33. Walker E. and Bujard, "Anomalous Temperature Behaviour of the Shear Elastic Constant C_{44} in Tantalum," *Sol. State Comm*., **34**, pp. 691-693, (1980).

34. Simmons G. and Wang H., Single Crystal Elastic Constants and Calculated Aggregate Properties: A Handbook, (The MIT Press, Cambridge, MA., 1971).

30. Private Communication, Albert Migliori, LANL.

36. Wagner W., de Reuck K. M., Schmidt R., Ewers J. , Stewart R. B., Jacobsen R. T., Oxygen International Thermodynamic Tables of the Fluid State-vol. 9, (Blackwell Scientific Publications, Oxford, 1987).

37. Tzikilis D. S., and Koulikova A. I., "Oxygen Compressibility Determination at Pressure to 1000 atm and Temperature to 400° C," *Zh. Phiz. Khimii*, **39**, pp. 1752-1756, (1965).

38. Belonoshko A. B., and Saxena S. K., "A Molecular Dynamics Study of the P-V-T Properties of Supercritical Fluids: CO_2, CH_4, CO, O_2 and H_2," *Geoch. Cosmochim. Acta*, **55**, pp. 3191-3208, (1991).

39. Schott G. L., Shaw M. S., and Johnson J. D., Shocked States From Initially Liquid Oxygen-Nitrogen Systems," J. Chem. Phys., **82**, pp. 4264-4275, (1985).

40. Mills R. L., Liebenberg D. H., and Bronson J. C., "Sound velocity and the Equation of State of N_2 to 22 Kbar," *J. Chem. Phys*., **63**(3), pp. 1198-1204, (1975).

41. Baer B. J., and Nicol M. F., "High-Pressure Binary Phase Diagram of N_2-O_2 at 295 K Determined by Raman Spectroscopy," *J. Phys. Chem*., **94**, pp. 1073-1078, (1990).

42. Fried L. E., and Howard W. M., "An Accurate Equation of State for the Exponential-6 Fluid Applied to Dense Supercritical Nitrogen," Accepted for publication in the November 1, 1998, issue of, *J. Chem. Phys*.

43. Abramson E. H., Slutsky L. J., and Brown J. M., "The Thermal Diffusivity tensor and Lattice Dynamics of β-Oxygen at High Pressure," *J. Chem. Phys*., **104**(4), pp. 5424-5428, (1996).

44. Roder H. M., "Transport Properties of Oxygen," *NASA Reference Publication*, **1102**, NSBIR 82-1672, (NASA-STIB, Washington, D.C., 1983).